Limiting Velocity & Acceleration Commands for Dynamic Control of a Large Vehicle

Martin Adams
School of Electrical & Electronic Engineering
Nanyang Technological University, Singapore
email: eadams@ntu.edu.sg

Javier Ibañez-Guzmán
SIMTech
71 Nanyang Drive, Singapore
email: javierg@gintic.gov.sg

Abstract

The effect of changing the input goal coordinates to a real vehicle's position control system is examined here. Such inputs provide motoring speed/torque signals, based upon local sensor information and the position of the global target, with little regard for the vehicle dynamics. In this article mobile robot path planning parameters are related to the application of correct, general control laws. The derivation of desired velocity/torque signals which feed a vehicle's speed/torque controller and conform to the velocity and acceleration limits of the vehicle is presented. A trajectory planner which produces correct displacement, velocity and acceleration profiles as a function of time is derived. These trajectories drive the vehicle to its target, while always keeping within the defined safe operating acceleration – velocity limits.

1 Introduction

In the past the issues of so called "higher level path planning" and "low level control" have usually been treated as separate issues [1, 2]. The philosophy presented here is that efficient mobile robot trajectory execution, can only result from a path planning algorithm which takes into account the 'lower level' motor dynamics of the vehicle concerned. The first aim of this article is to relate mobile robot path planning parameters to the application of a correct control law. Inspiration is taken from the work by Daniel E. Koditschek [3], as a control law for a large tracked mobile vehicle is derived from considerations of its total energy.

The second aim is to provide provably correct desired position, velocity and acceleration signals, so that the velocity and acceleration limits of the vehicle are never exceeded. This is done to make the controller's job easier in transferring desired target vectors into actual vehicle positions.

Section 2 begins by considering the energy of a vehicle moving under the influence of an artificial spring force, which pulls it towards its target. With the application of Lagrange's equation, provably correct desired speed or torque controllers are derived, which take into account the mass of the vehicle, as well as the imaginary, attractive spring constant and damping constraints. The controllers are also derived to account for limitations in a vehicle's speed or torque capabilities. It will be demonstrated that if a speed controller is used to guide a vehicle, then *acceleration* as well as position feedback should be used within the overall control system. Similarly a torque controller requires *velocity* as well as position feedback for correct position control.

To estimate the actual acceleration in the speed control system, section 3 demonstrates the use of an inertial measurement unit (IMU) and explains the transformations necessary to refer accelerations to a common navigational coordinate frame. Section 4 demonstrates the advantages of acceleration feedback and shows results which indicate a faster response than position only feed back systems, when a vehicle tracks step input changes.

Section 5 shows an experimental analysis to derive a safe operating area within which a vehicle's trajectory planner should operate within acceleration – velocity space. The step input analysis of section 4 is taken a stage further in section 6 as complete profiles of acceleration, velocity and position, which operate within the allowable acceleration – velocity space, are produced. Finally some results are shown which demonstrate the path following capabilities of each wheel, under the proposed algorithm.

2 Lagrangian Formalism

Here, a correct desired speed or torque signal for input into the corresponding speed or torque controller of a vehicle will be derived. The desired signal will be derived taking into account a vehicle's mass and an attractive force function towards its target. Consider a potential function ψ which assigns a scalar value to every position surrounding the mobile vehicle, and vanishes uniquely at the target with position vector

$\mathbf{x}_d$, i.e: $\psi(\mathbf{x}_d) = 0$. The imaginary potential energy of the mobile vehicle is ψ and its kinetic energy T is given by:

$$T = \frac{1}{2} M \dot{\mathbf{x}}^T \dot{\mathbf{x}} \tag{1}$$

where M represents the total mass of the mobile vehicle and $\dot{\mathbf{x}}$ its velocity vector. The total energy possessed by the vehicle is η given by:

$$\eta = \frac{1}{2} M \dot{\mathbf{x}}^T \dot{\mathbf{x}} + \psi \tag{2}$$

All non-conservative (dissipative) forces $\mathbf{F}_{ext}$ which act on the mobile vehicle are given by the Lagrange equation:

$$\frac{d}{dt}\left(\frac{\partial(T-\psi)}{\partial \dot{\mathbf{x}}}\right) - \frac{\partial(T-\psi)}{\partial \mathbf{x}} = \mathbf{F}_{ext} \tag{3}$$

which results in the expression:

$$\mathbf{F}_{ext} = M\ddot{\mathbf{x}} + \nabla\psi \tag{4}$$

In equation 4, $\nabla\psi$ is the *total force function* which is perpendicular to ψ at all points in space.

To arrive at a linear control law, a quadratic Hooke's law function can be used[1].

$$\psi = \frac{1}{2} K_1 (\mathbf{x} - \mathbf{x}_d)^T (\mathbf{x} - \mathbf{x}_d) \tag{5}$$

From equation 5:

$$\nabla\psi = K_1(\mathbf{x} - \mathbf{x}_d) \tag{6}$$

From Lagrange's equation 3, $\mathbf{F}_{ext}$ is by definition dissipative. To arrive at a controller which introduces damping into the otherwise oscillatory mass-spring system, let:

$$\mathbf{F}_{ext} = -K_2\ \dot{\mathbf{x}} \tag{7}$$

the negative sign indicating *dissipation*, $\dot{\mathbf{x}}$ the velocity vector of the mobile vehicle and K_2 a positive constant.

2.1 Speed/Torque Signal Derivation

The equilibrium force equation 4 can be used to derive a control law for a mobile vehicle. By substituting for $\nabla\psi$ (equation 6) and $\mathbf{F}_{ext}$ (equation 7) into the equilibrium force equation 4, using the operator $s = \frac{\partial}{\partial t}$ and rearranging, yields:

$$\dot{\mathbf{x}} = \frac{K_1}{K_2}\left[\mathbf{x}_d - \left(1 + s^2 \frac{M}{K_1}\right)\mathbf{x}\right] \tag{8}$$

Hence by considering the total energy of a mobile vehicle, when under the influence of an artificial spring type potential field, a control law results, namely that the desired velocity signal to the motors should be dependent upon both position and *acceleration* feedback of the vehicle.

We note that a *torque* control law can also be derived. If a motor produces a torque $\mathbf{T} = rm\ddot{\mathbf{x}}$ where r is the radius of the driving wheels and m the mass of the vehicle *carried by each wheel*, then [5]:

$$\mathbf{T} = rK_1\left[\mathbf{x}_d - \left(1 + s\frac{K_2}{K_1}\right)\mathbf{x} - \frac{1}{K_1}\nabla\psi_{rep}\right] \tag{9}$$

Equation 9 shows that if torque control is preferred, then the desired torque signal to the motors should depend upon both the position and *velocity* of the robot.

Equations 8 and 9 are general control laws since no assumptions about the vehicle's dynamics, in terms of transferring $\dot{\mathbf{x}}$ (or $\mathbf{T}$) into its position vector $\mathbf{x}$, have been made.

Before a realistic analysis of the controller suggested by equation 8 can be carried out, a further constraint must be imposed. The velocity signal $\dot{\mathbf{x}}$ can assume any values, dictated by $\mathbf{x}_d$, $\mathbf{x}$. In reality of course, a real vehicle cannot travel at any speed and will be limited to $\pm\mathbf{U}$ m/s say. We can take this into account, by replacing the linear amplifier with gain K_1/K_2 (equation 8), with a non-linear ideal saturation with the same gain but saturation levels of $\pm\mathbf{U}$. The same is also true for torque controlled motoring, in that the non-linearity would produce a saturated torque signal. With this inclusion, we can consider the response of the motor dynamics to unbounded velocity (or torque) signals, since the speed controller now restricts the motor inputs. Hence a realistic control loop which models the derived velocity control law is shown in figure 1.

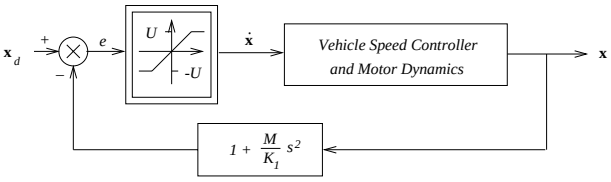

Figure 1: A non-linear control system representing the derived velocity control law. The linear region within the saturation element has gradient K_1/K_2.

Based on the vehicle's energy and a Lyapunov stability analysis, it can be shown that any realistic system[2] which adopts the controller of equation 8, and the speed/torque restrictions given above, will

[1] Khosla and Volpe have shown that irrespective of the chosen attraction function, it will approximate a *quadratic* cost function anyway, as the vehicle approaches its target [4]

[2] "realistic" meaning a system with low pass frequency characteristics.

be globally asymptotically stable, with respect to the given target vector $\mathbf{x}_d$ [5].

3 Estimation of Vehicle Accel.

The speed control algorithm of figure 1, requires an estimate of the actual acceleration vector $\ddot{\mathbf{x}}$. The use of a low cost, strap-down inertial measurement unit (IMU) is investigated for this purpose[3].

The implementation of figure 1 requires target vectors $\mathbf{x}_d$, the actual position of the vehicle $\mathbf{x}$ and its acceleration vector $\ddot{\mathbf{x}}$, to be defined in a common navigation frame. This requires a transformation between the vehicle frame, in which the accelerations from the IMU are measured, and the common navigation frame. Consider the navigation frame n represented by the orthogonal axes North (N), East (E) and Down (D) (figure 2). The second coordinate sys-

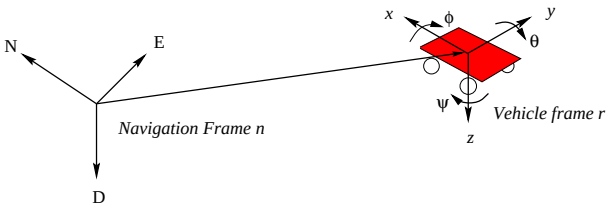

Figure 2: Relationship between the navigation frame n and the Vehicle frame r for transforming measured accelerations.

tem r is attached to the vehicle and is aligned with the axes of the IMU sensor.

The vehicle's orientation is given by the 3 Euler angles roll (ϕ), pitch (θ) and yaw (ψ). These angles are often derived from the integration of the measured angular velocities about the x, y and z axes in the vehicle's frame. The IMU used here has internal inclinometers, which provide the Euler angles directly, avoiding the need for numerical integration. If the order of rotations in frame r is taken about z followed by y followed by x, then the transformation matrix relating the measured accelerations to those in the navigation frame is given by [6]:

$$C_r^n = \begin{bmatrix} c\theta c\psi & -c\phi s\psi + s\phi s\theta c\psi & s\phi s\psi + c\phi s\theta c\psi \\ c\theta s\psi & c\phi c\psi + s\phi s\theta s\psi & -s\phi c\psi + c\phi s\theta s\psi \\ -s\theta & s\phi c\theta & c\phi c\theta \end{bmatrix} \tag{10}$$

where $c\theta = \cos\theta$ etc. The measurements from the IMU are the accelerations in the x, y, and z directions (frame r) and the angular inclinometer measurements are ϕ, θ and ψ.

[3]the IMU used here is a third generation marine motion sensor MRU-6, developed by Seatex, actually designed for underwater use. This is also fully functional for land based applications!

The acceleration vector due to gravity is assumed to act in the n_D direction and the centripetal acceleration due to the earths rotation is ignored since its value is practically immeasurable with a low cost strap down sensor, as used here [6]

4 Advantages of Acceleration Feedback

The advantages of the acceleration feedback term in figure 1 will now be demonstrated. Depending on the actual dynamics of the vehicle, its combination with the non-linear saturation can cause limit cycle oscillations. Adams has presented a detailed analysis of the limiting values of the gradient of the saturation K_1/K_2, necessary to avoid oscillation [5]. Knowledge of the vehicle dynamics for the large, tracked vehicle, used in these experiments, is limited and an experimental analysis is used to demonstrate the effectiveness of the acceleration feedback term. The left graphs in figure 3 show a simple step input to the steering unit, and resulting angular motion which would result if a perfect system were commanded to rotate through 22^o. A perfect response to this would

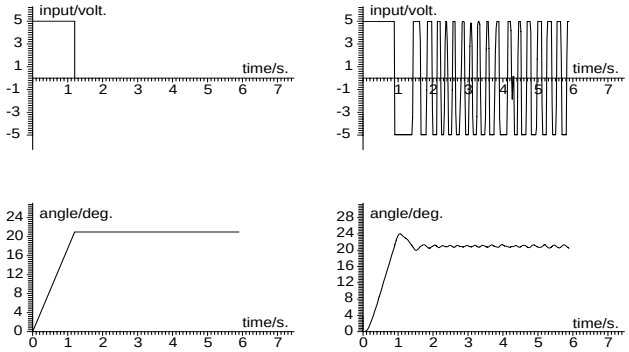

Figure 3: The response of a large tracked vehicle to target vector inputs. In the right graphs, a large gain K_1/K_2 was used to try and achieve a high response speed.

vary with time as shown in the bottom left curve.

The right graphs show the actual response of the vehicle for the chosen gain K_1/K_2 (chosen to achieve a high speed of response) when *no acceleration feedback* is used. The oscillation about the final angle is clearly visible and is an undesirable effect. If the gain K_1/K_2 is lowered, just below the limit for stable oscillations, the graphs in the left side of figure 4 result. It can be seen that the vehicle reaches its target, but rather slowly.

The graphs in the right side of figure 4 show the results of running the control algorithm of figure 1 with the same high gain used to produce the right graphs of figure 3. This time the acceleration feedback signal is also used, as suggested by the theoretical analysis in section 2. It can be seen that the desired change in

angular motion is reproduced almost perfectly as the angular change occurs at high speed with no oscillations. The initially "non-obvious" acceleration feedback term allows the control algorithm to be implemented to acknowledge the mass of the vehicle. The improvement in the tracking performance is demonstrated.

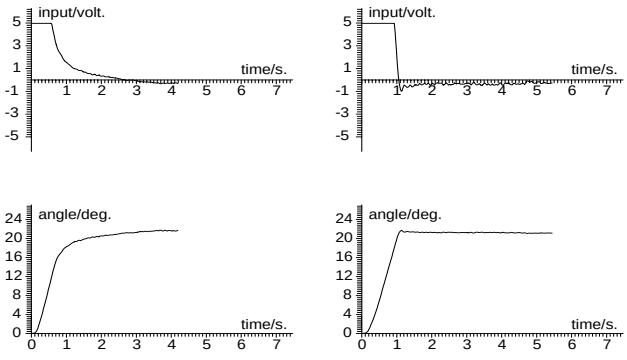

Figure 4: Slow and fast asymptotically stable response of the tracked vehicle. The left hand graphs show the result when $K_1 = 120$ and $K_2 = 1.0$. The vehicle asymptotically approaches its target but the response speed is slow. The right hand curves demonstrate the advantage offered by the acceleration feedback as the response speed is increased.

5 Maximum Accel. – Vel. Relations

If ΔT is the target vector update time, then:

$$\ddot{\mathbf{x}} \approx \frac{\dot{\mathbf{x}}(k) - \dot{\mathbf{x}}(k-1)}{\Delta T} \leq \ddot{\mathbf{x}}_l \qquad (11)$$

The velocity vector $\dot{\mathbf{x}}$ found in part 2, now referred to as $\dot{\mathbf{x}}(k)$ must be limited to:

$$\dot{\mathbf{x}}(k) \leq \ddot{\mathbf{x}}_l \Delta T + \dot{\mathbf{x}}(k-1) \qquad (12)$$

where $\ddot{\mathbf{x}}_l$ is the allowable limiting acceleration for the vehicle. This limit i, in general, a function of the current vehicle's velocity.

The vehicle used in this analysis was powered by a large diesel IC engine, which is typically characterised by a torque – power curve. Typical diesel engines have a torque/force velocity curve which rises with decreasing velocity, such as that shown in figure 5 for a vehicle with 4 gears [7]. To obtain the required acceleration versus velocity operating chart for such a vehicle, an estimate of the tractive force at the wheels/tracks must be determined. For real vehicles this analysis is often idealised and prone to large numerical errors, for example if a change of lubricant or a mechanical component has occurred [7]. Therefore tests were carried out to determine

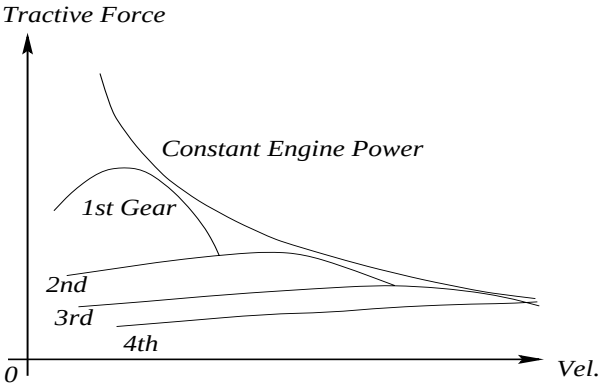

Figure 5: A typical tractive force – velocity curve for a diesel vehicle with 4 gears.

approximately the available forward acceleration at different vehicle speeds. The vehicle was manually driven to maintain a constant speed, and at a particular point in time, full throttle was applied, to attain maximum acceleration, which was then measured. These tests were repeated on flat terrain, in a forward and reverse direction, and on inclined terrain. The available acceleration for each tested speed is shown in figure 6[4]. These curves represent the *characteristic* curves required for smooth path production with reachable velocities and accelerations.

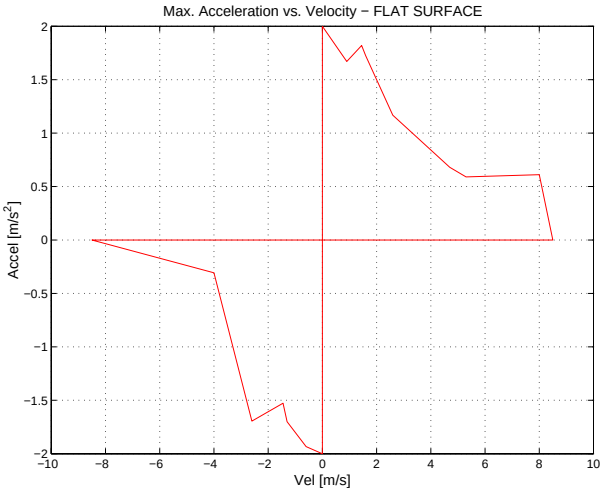

Figure 6: Terrain: **Flat Ground**; Motion: Forward and Reverse.

The next step is to mathematically categorise figure 6, in a conservative sense, so that new velocity vectors are produced by the controller, which always

[4]Similar charts were recorded for up hill and down hill motion, with obvious decreases and increases in available accelerations.

obey inequality 12, where $\ddot{\mathbf{x}}_l$ is the maximum acceleration available, at speed $\dot{\mathbf{x}}(k)$, determined from graph 6.

6 Restricted Accel. – Vel. Trajectory Generation

Section 5 has provided an estimate of the safe operating area in acceleration – velocity space, within which all paths for each of the vehicle's wheels/tracks should be planned. Figure 6 shows the general form of the safe operating area. It should be noted however, that if the tests are repeated, or if changes to the vehicle are made (eg. new mechanical components or even a change of lubricant), the form of the graphs remains, but the numerical limits can change significantly (changes of up to 40% were noted during experiments). Therefore, based on the figures, a simplified and conservative operating area which limits the maximum acceleration and velocity to only 60% of those found by experiment in figure 6 was used. This is shown by the solid lines in figure 8.

Various trajectory generation techniques exist for planning smooth paths between two points, subject to velocity, acceleration, jerk and higher order time derivative limits [8]. Once a target vector is generated by the navigation algorithm, the individual path profiles for each track are calculated from the vehicle kinematics. Instead of analysing the control system with step inputs, correct profiles (displacement, velocity and acceleration versus time) are calculated such that the safe operating area of figure 8 is used as optimally as possible. To make optimum use of the safe operating area[5], profiles in acceleration – velocity space which follow the Amax - Vmax line should be generated. The problem here is that profiles with infinite jerk result, a quantity which is known to produce oscillations [10].

Since new target vectors $\mathbf{x}_d$ are generated at regular intervals, the initial experiments here, produce simple profiles with *constant jerk*. These profiles are shown in figure 7, from which the velocity profile is used as the $\dot{\mathbf{x}}$ signal in figure 1.

If the acceleration profile from figure 7 is plotted against the velocity profile[6] on the operating chart of figure 8, curves (shown dashed and dot-dashed) result below the acceleration – velocity limit lines. In figure 8, the profiles have been generated to achieve the required displacement, and to touch the Amax – Vmax limit line once. Subject to the conditions of constant jerk, this trajectory produces an optimal time path within the limits of the safe operating area.

[5] i.e. produce displacement profiles which reach the target in minimum time [9]

[6] i.e. eliminating the time parameter.

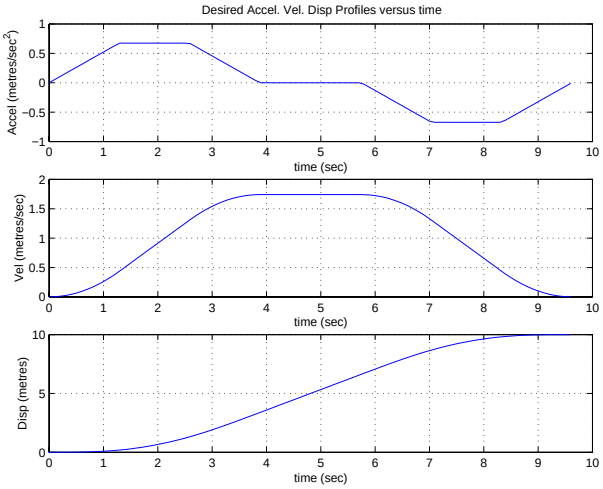

Figure 7: Acceleration, velocity and displacement profiles produced under constant jerk conditions.

The advantage of this technique is that profiles can always be generated to meet the required target vector $\mathbf{x}_d$ and that limits can be applied to limit the acceleration and/or velocity further, if deemed necessary by the navigation algorithm. This is demonstrated in figure 8 where a further profile in acceleration – velocity space is shown (dotted curve) with restricted acceleration and velocity.

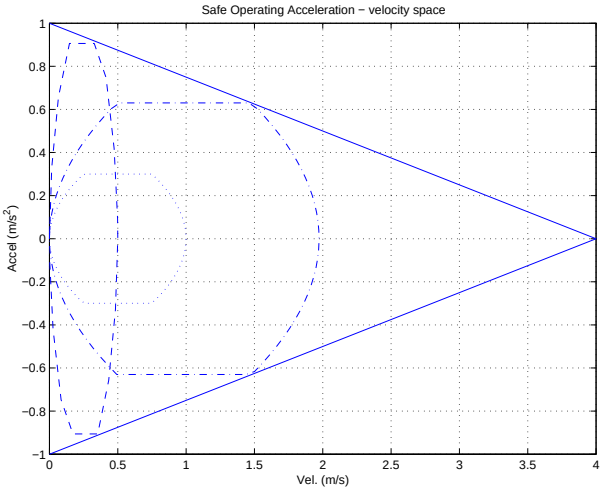

Figure 8: Safe operating accel. – vel. space for all vehicle path profiles. The dashed curve shows a trajectory with limited vel. (0.5 m/s). The dashed - dot curve shows a trajectory with limited accel. (0.63 m/s^2) and the dotted curve shows a trajectory with limited vel. (1.0 m/s) and accel. (0.3 m/s^2).

7 Results

Figure 9 shows the *actual* trajectory followed by one track, for the desired accel. – vel. – disp. profile of figure 7. In this test *no* acceleration feedback was

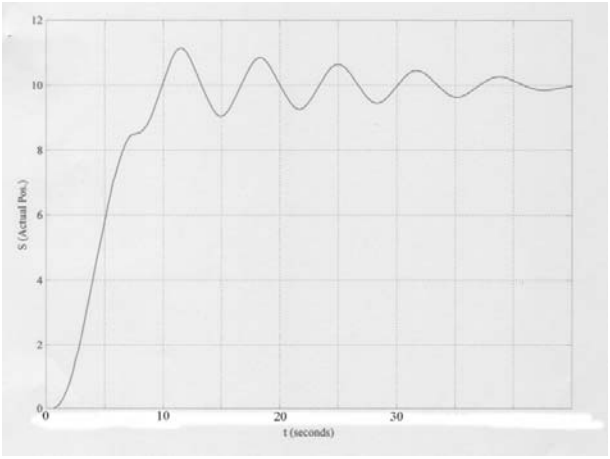

Figure 9: Single track response to the desired velocity trajectory input of figure 6, when no acceleration feedback is used.

used, and although the trajectory following phase itself shows a good performance, a clear damped oscillation about the final position is evident.

Figure 10 shows the results of the same test, when acceleration feedback was used. A small oscillation

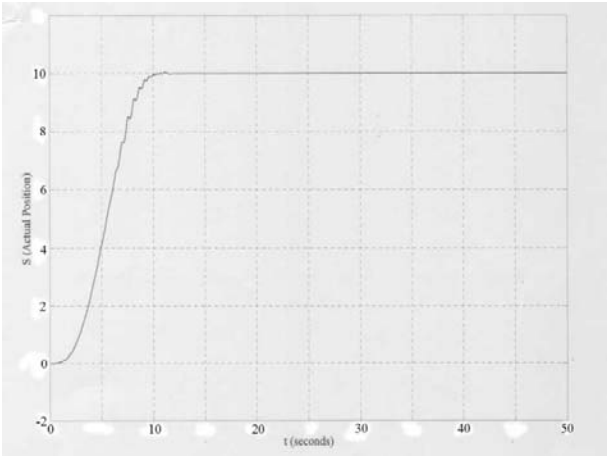

Figure 10: Single track response to the desired velocity trajectory input of figure 6, when acceleration feedback is used.

is evident in the braking phase of the displacement profile, as the mass of the vehicle is used to correct the feedback signal. Upon reaching the target the track shows minimal recorded oscillation.

8 Conclusions

Based on considerations of the kinetic and artificial potential energy of a vehicle, provable desired speed/torque control algorithms have been designed, and a speed control system has been tested, using both step and derived smooth velocity profile inputs. The acceleration feedback term (in the case of the speed control algorithm) has shown its ability at reducing oscillations in position for *both* step and velocity-time trajectory inputs. A faster possible response time to step inputs was also noted.

A safe acceleration – velocity operating chart was experimentally derived which lies within the torque – velocity characteristic curve of a given vehicle. A trajectory generator was defined which produced constant jerk profiles in acceleration, velocity and displacement which guaranteed that the desired input signals would never exceed the acceleration – velocity limits of that vehicle.

The issues addressed here have shown, that a vehicle's control system can operate much more efficiently if the desired inputs are derived and conditioned to take into account a vehicle's mass, acceleration and velocity limits.

References

[1] E. Freund and R. Mayr. Nonlinear path control in automated vehicle guidance. *IEEE Trans. Robotics and Automation*, 13(1):49–60, 1997.

[2] Z. Shiller and Y.R. Gwo. Dynamic motion planning of autonomous vehicles. *IEEE Trans. Robotics and Automation*, 7(2):241–249, 1997.

[3] Daniel E. Koditschek. *Robot Planning and Control Via Potential Functions - from the Robotics Review.* The M.I.T Press, 1989.

[4] P. Khosla and R. Volpe. Superquadric Artificial Potentials for Obstacle Avoidance and Approach. In *IEEE Trans. Robotics and Automation*, pages 1778–1784, 1988.

[5] M. D. Adams. Stability and high speed convergence in mobile robotics. *IEEE Trans. Robotics and Automation*, 15(2):230–237, 1999.

[6] Billur Barshan and Hugh F. Durrant-Whyte. Inertial navigation systems for mobile robots. *IEEE Trans. Robotics and Automation*, 11(3):328–342, 1995.

[7] Thomas D. Gillespie. *Fundamentals of Vehicle Dynamics.* Society of Automotive Engineers, Inc., 1992.

[8] Winston Nelson. Continuous-curvature paths for autonomous vehicles. In *IEEE Trans. Robotics and Automation*, pages 1260–1264, 1989.

[9] A. Meystal, A. Guez, and G. Hillel. Minimum time path planning for a robot. In *Proc. IEEE Int. Conf. Robotics and Automation*, page 1678, 1986.

[10] John J. Craig. *Introduction to Robotics: Mechanisms and Control.* Addison-Wesley, 1986.